Fall Current Characterization Models

Thomas W. Kotowski

VXPhysics.com

4813 Skyline Blvd.
Cape Coral, FL, 33914-6533
239-540-7340
FAX 239-540-7340
tkotowski@comcast.net

Abstract - **Many common inductive loads, in particular, passenger car, engine control, electromechanical linear actuators, are magnetically saturated. Experimentally, it is found that the "inductance" of these actuators decreases approximately linearly with increasing load current. Our goal is to characterize the saturation inductance behavior of these actuators, within a few percent accuracy, using the minimum number of load characterization parameters. The fall current saturated inductance of these loads can be compactly modeled with linear dynamic inductance. Compact models for extremes of operation and criteria for applicability of the models are developed. Using current/time shifting, the model accuracy and accommodation of complexity can be increased. The increased accuracy of load characterization can be exploited for the reduction of silicon area and associated cost of the semiconductor inductive load drivers.**

Mathcad Modeling Files

http://www.leapcad.com/Actuator/3_Point_Dyn_Mag_BiSat.pdf

http://www.leapcad.com/Actuator/3_Point_Dyn_Mag_BiSat.mcd

I. INTRODUCTION

These Inductance Saturation Models were developed to facilitate the assessment of an engine controller power FET's safe operating area (SOA) margin. The minimum number of model parameters was essential for ease of use and acceptability by our automotive customers. Assuring the reliability of a power device in an inductive switching application requires some determination that the junction peak transient temperature during turnoff is less than some critical value. The thermal time constant of the FET is on the order of the falltime of the inductance. Thus, the junction peak transient temperature is critically dependent on the rate of falloff of the peak power pulse during the first half of the inductive turnoff. For the saturated inductors we evaluated, static inductance predicts an unrealistic fall current curve, with a di/dt that can differ from the actual rate by a factor of three. The error in estimation of the peak transient temperature rise, for the drivers we evaluated, based on the static inductance model, is typically +30%, but can range from about -10 to +40%. The goal is to exploit the compact model for driver silicon area and its associated cost reduction.

II. COMPACT DYNAMIC INDUCTANCE SATURATION MODELS

We will consider four models of "effective" inductance: Conventional static, Linear Saturation, Bi-effective, and Bilinear Saturation. We will look at the limitations of the Linear Model and ways to extend its applicability to cases of extreme saturation. It will be shown that the applicability of the linear model is approximately determined by the value of an energy ratio, n_{Em}. This energy ratio decreases as the low current "tail" of the fall current versus time increases. Saturation of our inductors ranged over a factor of three in relative energy content, n_{Em}.

Magnetic saturation of an automotive inductor can result from a number of factors. For example, a minimum cost (maximum performance) design may specify the minimum amount of magnetic material (minimal mass) or an inductive load may be subjected to fault condition, such as voltage doubling during automotive jump-start.

Figures 1 and 2 depict "saturation" for two automotive electromechanical actuators measured at 16V: a reverse lockout solenoid and a fuel injector, respectively. The straight line in each plot is the least squares fit, linear regression line to the high current region. **The plots reveal that inductance (i.e. dynamic inductance) is not constant,** but that the peak current value (right edge of plots) is typically 90% less than the low current value. (Note that the normal direction of falloff time, that is, left to right, is reversed in these plots. The corresponding fall current - time plot normally starts with the peak current on the left, at time zero, and with increasing time, then decays toward the right.)
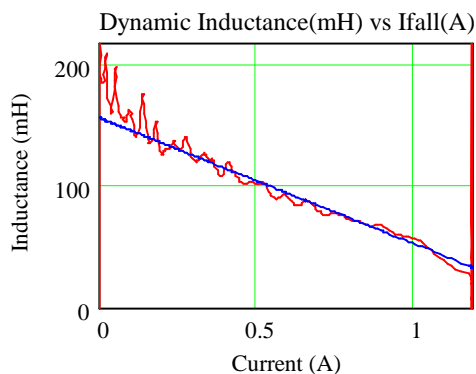

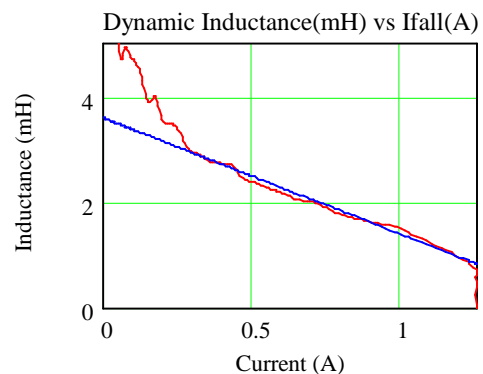Fig. 1. Reverse lockout solenoid inductance, $\Lambda(i)$.

Fig. 2. Fuel injector inductance, $\Lambda(i)$.

A. Conventional or Static Inductance - Limitations

A fundamental definition of conventional or static inductance is the ratio of magnetic total flux linkage, Φ_{tot}, to current (i.e., $L = \Phi_{tot}/i$) [1]. During saturation at high current, the *incremental* increase of flux decreases and consequently, the flux to current ratio, or inductance, decreases. To better quantify this behavior, we introduce a quantity called dynamic inductance [2,3], symbolized as Λ, which we define as the *differential* change of flux with current (i.e., $\Lambda = d\Phi_{tot}/di$). For an electromechanical system, dynamic inductance is a function of clamp voltage, peak current and the components of the analogs of inertia, plunger velocity, friction, spring constant, wire distribution flux, differential permeability (dB/dH), etc.

The induced voltage (emf) of an actuator with plunger moving in the x direction is found from the time rate of change of flux (i.e., emf $= d\Phi_{tot}(x,i)/dt$). Applying this to our definition of static inductance, for the case of saturation, gives emf $= Ldi/dt + \partial\Phi_{tot}/\partial x * dx/dt$. For dynamic inductance $d\Phi_{tot} = \Lambda\,di$ and thus emf $= \Lambda\,di/dt$. By definition, dynamic inductance is directly observable from the emf and di/dt, while static inductance for saturation has the velocity dependent (back emf) term $\partial\Phi_{tot}/\partial x * dx/dt$.

B. Linear Saturation Model – Inductance

We will use **linear saturation as a first order empirically based model** for *moderate* saturation of any inductor. We observe that the falloff of the average current with time is monotonic. Thus, there is a one-to-one correspondence between falloff current and time. From the previous plots, we discover that flux saturation of actuators that are *heavily* saturated is also approximately linear with current in the high current region at the right. We use these two observations to construct a first order empirical model of saturated dynamic inductance, represented as $\Lambda(i) = \Lambda o - k\,i$, where Λo is the dynamic inductance at zero current (low current "tail" inductance) and k is the constant slope of decreasing dynamic inductance with current. This also meets our requirement for a model with the minimum number of parameters. From this model, the peak current (minimum inductance) saturation end-point, Λ_{Ipk}, is equal to $\Lambda o - k\,Ipk$, where Ipk is the peak current. For heavy saturation of magnetic materials, Λ_{Ipk} approaches its fully saturated dynamic inductance as a lower limit. (The nomenclature we use is summarized near the end of this paper.)

Let's make some rough generalizations to explore the behavior of dynamic inductance. For an unsaturated magnetic core, the change of flux with current is constant, and in this case, Λ reduces to the static inductance value, L. For inductors in general, the average value of the actual dynamic inductance with respect to the endpoints, $(\Lambda o + \Lambda_{Ipk})/2$, is roughly equal to the (effective) static inductance. For heavy linear saturation, such as in automotive actuators, the value of Λo is roughly about twice as large as the effective (See second paragraph below) static inductance.

1.) Derivation of Fall Current Equation, $n_{Em} \geq 0.5$: A voltage clamp is commonly used with integrated circuit inductive driver applications [7]. We will use the typical application circuit in Figure 3 to characterize the fall behavior of an inductive load. When the switch is turned off, the inductor rings the Vds voltage up to the fixed clamp voltage, Vds_{clamp}, to keep the initial current constant at Ipk. We will refer to these current, voltage, and resistance variables as "clamp variables." The solid curved line, If_{dat}, in Figure 4 shows data for the fall current of a saturated inductor, an automotive PWM solenoid at 16V.

The *effective* inductance, Leffective, has been defined as the static inductance that matches an amount of fall energy, E_m, equal to that *dissipated in the voltage clamp* (i.e., fall time

integral of Vds_{clamp} x icoil). The straight solid line in Figure 4 shows the current predicted from the effective inductance model. For this inductive load and our other saturated samples, the static model is clearly amiss. Typically for our saturated samples, the static model has an error of
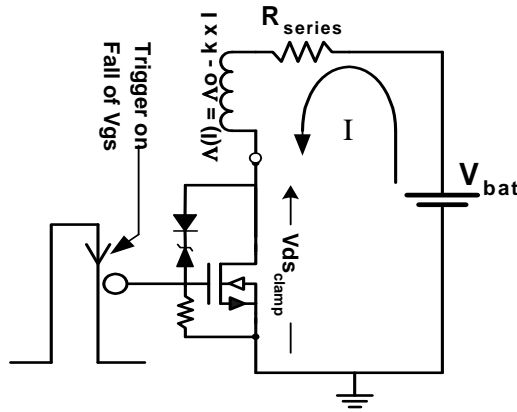
Vds Clamp

Fig. 3. Characterization circuit.

Actual fall current, If_{dat}, for an actuator is poorly modeled by a constant inductance, L_{eff} (black), but accurately by dynamic inductance models for either tm or Em (see below and Mathcad file models).
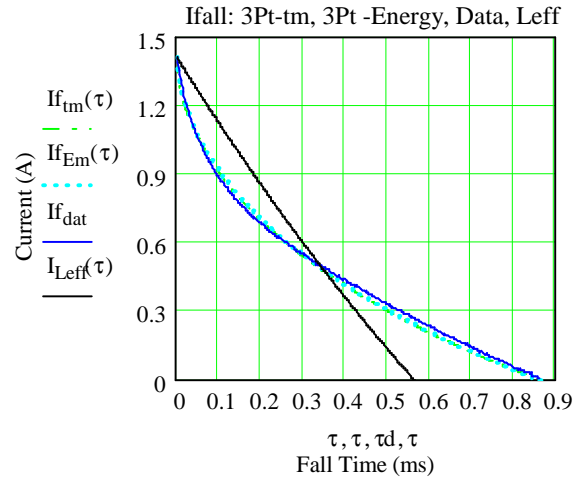

Fig. 4. PWM solenoid fall current.

~30%, both at the point of maximum fall current deviation and for the fall time.

The loop equation for the linear saturation dynamic inductance fall current model is:

$$\frac{di}{dt} = \frac{V_{Bat} - Vds_{clamp} - R_{series} * i(t)}{\Lambda o - k * i(t)} \tag{1}$$

This is a nonlinear equation that is integrable[4].   Integrating, rearranging, and solving for the current gives a solution with the general form i(t) = (Λo - Λ(t))/k, where Λ(t) is the dynamic inductance. However, Λ(t) is given in the terms of the Lambert W function [5]. This exact linear solution with the Lambert W function is not very satisfactory. The solution does not give a good match to the empirical fall current data (it is larger than the data at high currents), the Lambert W function does not permit explicit solution for the its two Λo and k parameters and the numerical solution is often physically unrealistic.

We need a mapping function to accommodate small nonlinearities of inductance implicit in the actuator fall current data and yet provide a model current with linear inductance.

A first order approximation to the Lambert W function is a power law function with exponent less than 1. The fall current can thus be approximated by the power function expression $Ipk [1-(t/t_{fall})^n]$.   This provides an exact match to the peak current Ipk and to the current fall time, t_{fall}. The value of this new parameter, n, can be found by demanding a match either to the solenoid's dissipation energy, Em, (n_{Em}) or to some high current point at an associated time tm (n_{tm}). See Appendix for the expressions for n. This decay function always gives a physically realistic solution. The resulting model currents (shown in Fig. 4) are $If_{Em}(t)$ and $If_{tm}(t)$, respectively.

The resulting simple power law current, i_{nlaw}, provides a better match for the actual fall current data. This power function manifests a decay of inductance that is slightly nonlinear with current and it is complementary to the Lambert function, i.e., its current at high current is less than the empirical data.

We can remedy the defects of the above exact Lambert W function solution. We demand a realistic fall current solution, exactly linear in inductance (with parameters Λo and k), which satisfies the loop equation, and matches the fall curve data exactly for at least three points.

We will use the power function to bootstrap to the desired solution by substituting i_{nlaw} for $i(t)$ just in the Rseries $i(t)$ term in the linear differential loop equation. The power law expression makes the above linear inductance differential loop equation integrable into a form that allows an algebraic solution. This yields the self-consistent algebraic solution for the dynamic linear inductance fall current in terms of characterization parameters Λo and k, given by:

$$i_\Lambda(\Lambda o, k, t_{fall}, t) = \frac{\Lambda o - \Lambda(\Lambda o, k, t_{fall}, t)}{k} \tag{2}$$

$$\Lambda(\Lambda o, k, t_{fall}, t) = \sqrt{\Lambda o^2 - 2\ k * \left[\Lambda o\ Ipk - \frac{k}{2} Ipk^2 + v_{bzr}(t_{fall}, t)\right] * t} \tag{3}$$

$$v_{bzr}(t_{fall}, t) = V_{Bat} - Vds_{clamp} - Rseries\ Ipk \left[1 - \frac{1}{1+n}\left(\frac{t}{t_{fall}}\right)^n\right] \tag{4}$$

(We will use t_{fall} later as a variable in the bilinear model for more complex saturation situations.)

This time domain equation has the same general form as the Lambert W solution and also as our saturation model, $i = (\Lambda o - \Lambda)/k$. (See Figs. 7 and 8.)

2*.) Find Parameters - Three-Point Match (Ipk, t_m or E_m, t_{fall})*: Given the Ipk, t_{fall}, and the clamp variables, we can find the value of Λo either by matching a high current point of interest, I_m, or by matching the fall energy, E_m, *dissipated in the clamp*, giving the values Λo_{tm} and Λo_{Em}, respectively. Analogous to Leffective, but with a greater degree of current matching accuracy, Λo_{Em} is the effective dynamic linear inductance.

The i_Λ equation can be solved directly for Λo in terms of a current match point, I_m, and its associated time, t_m. It is convenient to match the current at some predetermined fixed point ratiometric to the peak current. Select the point (~0.70 x Ipk) which tends to give the best match to the mid-high current region. Then the required data point is just the time, t_m, for the current to reach 0.70 x Ipk. This solution for Λo, designated as Λo_{tm}, is shown in the Appendix. This solution typically has a fall energy that is within 5% of the measured clamp energy, E_m.

The value of Λo_{Em} can be found by matching the energy calculated from Λo to the measured value E_m. This can be done with a Solver (Excel, Mathcad, and others) or by tweaking the value of Λo_{tm} to match the energy, as shown in the following paragraph. Mathcad is the easiest way to implement this Solver. This Mathcad procedure is illustrated in the Appendix.

Let's look at an alternative to a Solver. The value of Λo_{tm} can be used as an initial point for an energy corrected approximation to Λo_{Em}; call it Λo_{Em-tm}. Then Λo_{Em-tm} can be found by taking differentials of the theoretical stored energy (see the paragraph after next) with respect to Λo. This gives an approximate value for Λo_{Em} based on Λo_{tm} that is equal to $\Lambda o_{tm} - 0.85$ x $6(E_m - E_{tm})/Ipk^2$, where E_{tm} is the fall energy calculated from the integral of $Vz * i_\Lambda(\Lambda o_{tm}, ko_{tm}, t_{fall}, t)$ over t_{fall}. The calculation for Λo_{Em-tm} is shown in the Appendix. An associated tweaked value of k, $k(\Lambda o_{Em-tm}, t_{fall})$ (refer to the Appendix), then needs to be calculated.

The match from Λo_{Em-tm} to Λo_{Em} is generally within 5%. If $n_{Em} \geq 0.5$, a match within a few tenths of a percent can be obtained with a second iteration, using the first value of Λo_{Em-tm}

and its associated value of k and fall energy. As demonstrated by the plot of the automotive PWM solenoid current at 16V ($n_{Em} = 0.5$) in Figure 4, both the central current point and energy methods, give a good current match, If_{tm} and If_{Em}, respectively, to the overall current data. Typically, if $n \geq 0.5$, half of the high current model points are within ~2% of the current data.

The power supply adds energy in addition to that stored in the inductor during the fall time. The stored energy is typically about 85% of E_m. It can be shown that the stored theoretical linear saturation energy is $\frac{1}{2} \Lambda o_{Em} Ipk^2 - \frac{1}{3} k_{Em} Ipk^3$. The effect of the two opposing terms is, for heavy saturation, that the energy, E_m, increases more like linearly, rather than as the square of Ipk, as in the case of static inductance.

C. Linear Saturation Limited Model, Peak Current - Zero Inductance Solution Λo_{zpk}, $n_{Em} \sim 0.5$

Consider the case of a heavily linearly saturated (~ 90% Λo decrease) inductor. A hypothetical *linear* saturation limit is when the high current saturated inductance decreases to zero. Without any knowledge of t_{fall}, given just this hypothetical zero inductance condition, the measured energy, and the clamp conditions, and we can solve the Esw energy equation for Λo. The value of k is then equal to $\Lambda o_{zpk}/Ipk$, and the fall time, $tfall_{zpk}$, is estimated from the expression for $tfall_{encoded}$, shown in the Appendix.

III. LIMITATIONS, $n_{Em} < 0.5$: FULLY SATURATED REGION AND COMPLEXITY

A. Extreme Saturation, Energy Ratio, $n_{Em} < 0.5$

The Appendix shows that n_{Em}, equals the energy ratio $1/(Ipk\ Vds_{clamp}\ t_{fall}\ /Em - 1)$. This energy ratio is a rough measure of the degree of (saturation causes the relative stored energy to be reduced). (The area under the If_{dat} curve in Figure 4 is measured to be one-third the rectangular Ipk x t_{fall} area and thus it has a n_{Em} value of 1/2. This corresponds to a moderate to heavy degree of saturation.)

We now consider the linear heavy saturation limit. The energy ratio, n, is the exponent of the falloff of the power law approximation to the actuator falloff current. As the energy ratio n decreases, the "tailing" of the falloff current with time increases. It has been found that the linear saturation model will overestimate heavy saturation, and show increasing error, as the inductor's energy ratio drops below 0.5. As noted below, that is often the result of additional phenomena occurring, making the fall current behavior more complex than that of the simple linear model.

B. Deviations from the Linear Model, $n_{Em} < 0.5$

Figure 5 is a plot of the saturation of a skip shift solenoid at both the nominal 16V (dotted lines, $n_{Em} = 0.5$) and extended double battery 26V (solid lines, $n_{Em} = 0.35$). The lowest solid and dotted lines are regression lines to the extended high current region. These lines transition, or cross at about 0.8A. This point is denoted as I_{tran}. (This point is somewhat arbitrary. For the case of our sample automotive actuators, this transition current level roughly corresponds to the peak current level at a 10V supply voltage.) The corresponding time is t_{tran}. The upper lines are $\Lambda(i)$ from our model. The plots show that by extending the high current region, the overall saturation increasingly deviates from our linear model as the supply voltage is increased beyond the normal operating range.

Figure 5 shows that "nonlinear" dynamic inductance versus current saturation at low currents increases the overall slope relative to the high current region and causes the model inductance at the peak current, Λ_{Ipk}, for a least squares fit linear regression line, to be negative.
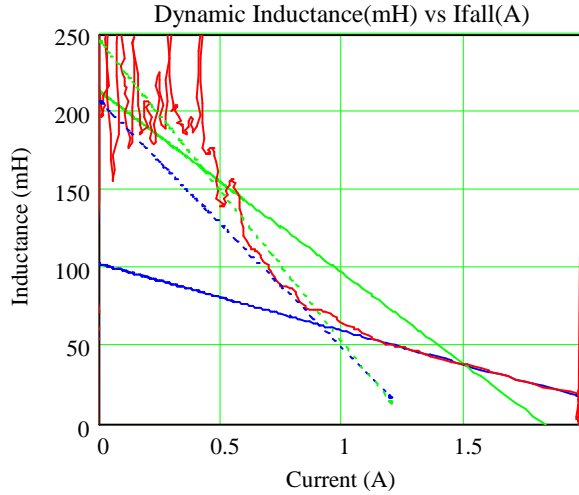
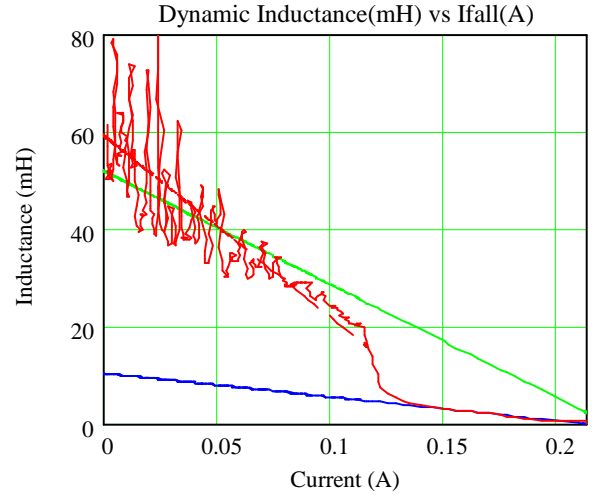Fig. 5. Skip shift solenoid @26V inductance, $\Lambda(i)$.

Fig. 6. A/C clutch relay inductance, $\Lambda(i)$.

Negative inductance is physically unrealistic. If Λ_{Ipk} is less than zero, the linear solution, i_Λ, is not valid and does not concurrently match the peak current and the central current/energy. This imposes a maximum value for Λo of 2 t_{fall} {$Vds_{clamp} - V_{Bat}$ + Rseries Ipk [n/(1+n)]}/Ipk. The value of Λ_{Ipk}, or Λo versus the above maximum, should be checked for validity if n is close to, or less than, one half.

C. Complexity: Power Law Fit – Three Point Match, Ipk, t_m or E_m, t_{fall}

Relays display two distinct magnetic states, characterized by two distinct dynamic inductance slopes. Their dual slope behavior requires additional model parameters and thus is more complex to model. Figure 6 is a "saturation" plot of an automotive air conditioner clutch relay at 16V (n_{Em} = 0.30). The broken and lowest lines are the regressions to the relay's low current (open magnetic path) and linear high current (closed magnetic path) portions, respectively, and the top line is the linear analytic model dynamic inductance, which overestimates nonlinear "saturation."

There are some nonlinear, slow decay, cases in which the nonlinear power law function Ipk $[1-(t/t_{fall})^n]$ can provide a better fit than the Three-Point Linear Saturation Model. The power law function is not an explicit model for variation of inductance with saturation, it is a convenient general curve fit. For a quantitative comparison, the time averaged dynamic "inductance" for If_n is (Vds_{clamp} - V_{Bat} + Rs Ipk n_{Em}/2) tf /{Ipk n_{Em} (2 - n_{Em})}.

IV. BI-EFFECTIVE INDUCTANCE TEST STANDARD

A. Extracting L_{Ipk} and L_{tail}

The representative extended voltage inductance versus current plot of Figure 5 and also the Figure 6 relay plot suggest that the solenoid current can be decomposed into two regions: a peak current region and a low, or tail, current regions. The electrical dynamics in these regions are roughly simulated with a parallel pair of the series combination of a resistance and an inductance. This pair consists of a small (peak current) inductance with a fall time equal to t_{tran} ($\propto L_{Ipk}/R_{Ipk}$) and a larger inductance with a (tailing) fall time ($\propto L_{tail}/R_{tail}$). The faster discharge L_{Ipk}/R_{Ipk} leg requires a power diode in series with it to block reverse current flowing through it after its fall time, t_{tran}, from the L_{tail}/R_{tail} leg.

Define the bi-effective pair inductance as the inductance pair that matches the total energy dissipated in the voltage clamp by the actuator and also matches the fall energy dissipated in the clamp by the actuator during the fall from the peak current to the current at I_{tran}.

There are four unknowns, (a pair of resistances and a pair of inductances) for which we establish the four requirements: the paralleled series (total) resistances must equal Rseries, the total fall energy must equal E_m, the fall time for the (peak region) current through L_{Ipk}/R_{Ipk} must equal the time t_{tran}, and the FET dissipation energy from the parallel L/R pair from the peak current to I_{tran} must equal that of the actuator. (If we get a solution such that the fall time associated with L_{tail}/R_{tail} is much larger than that of the actuator, we add the arbitrary constraint that L_{tail} is ≤ 3.5 x L_{Ipk}.)

Figure 7 shows a plot of the skip shift bi-effective fall current, If_{bieff}. (For reasons, which will be made clear below, we label the transient point $I_{tran}@t_{tran}$ as $I_{mask}@t_{mask}$.)

V. BILINEAR SATURATION MODEL

A. *Current/Time Shift Partitioned Linearization*

The bi-effective static inductances are a much better model than just the effective inductance. However, the bi-effective characterization parameters are somewhat arbitrary and they are still an approximation to, and not a realistic model for, magnetic saturation. Figures 5 and 6 reveal that an accurate and realistic characterization of the over-voltage solenoid and relay requires the separation and extraction of the nominal versus the full saturation and the open magnetic path versus the closed magnetic path regions, respectively. We wish to partition the inductance curve in Figure 5 into two regions: an extended high current fully saturated region and a low to nominal current region.

1.) Extended High Current Fully Saturated Region: An easy way to do this is to null out, or mask out, the low to nominal current region by current level shifting. Because our model is linear with respect to current, we can subtract a current level, I_{mask}, from our current data, apply our linear model, and then add this current level back after we calculate the solution parameters for the shifted current $i_\Lambda(\Lambda o, ko, t_{fall}, t)$. For example, we take the current data shown in Figure 7 and subtract an I_{mask} level of 0.8A. We choose 0.8A because it roughly corresponds to the transition to the linear portion of the high current versus time plot. The peak current is now 0.8A less and the fall time, or time for the current to go to the new zero level, is now the time corresponding to the I_{mask} data point. We designate this time as t_{mask}.

Based on this new truncated peak current (Ipk - I_{mask}), the truncated high current fully saturated region energy (or match current) and new fall time, we can calculate the shifted dynamic inductance parameters Λo_H and k_H, for this new high current data from the Λo and k equations in the Appendix. (In general, to compensate for the reduced "peak" current, the initial series resistance must be increased by a factor of Ipk/(Ipk – I_{mask}) to maintain the original un-shifted voltage drop for calculation of Λo_H and k_H. If there is appreciable voltage variation, the average values of V_{Bat} and Vds_{clamp} restricted to the high current region should also be used.) For this device we find that the energy ratio, n_{Em}, for the transformed upper current region is 0.58.

2.) Low Current Nominal Region: For the remaining low current nominal portion, the peak current is now I_{mask} or 0.8A, and the new low current fall time is our original fall time minus t_{mask}. From this and either the low current region energy or a current match point, we calculate the time shifted dynamic inductance parameters Λo_L and k_L. (In general, the initial series resistance is increased by a factor of Ipk/I_{mask} to scale for the revised peak current I_{mask}. If there is appreciable voltage variation, low current values of V_{Bat} and Vds_{clamp} may also be needed.) For this device, the energy ratio, n_{Em}, for the low current region is 0.66.
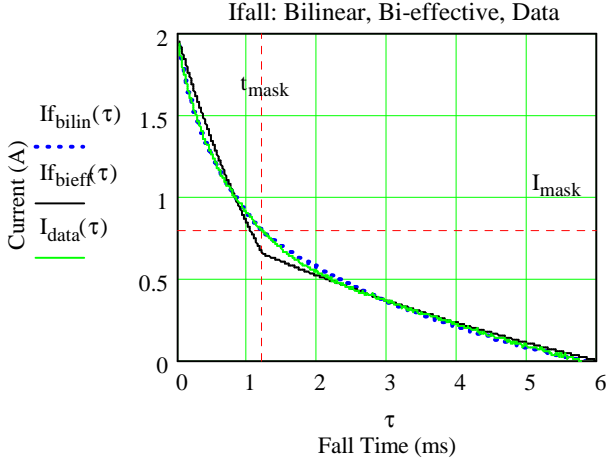
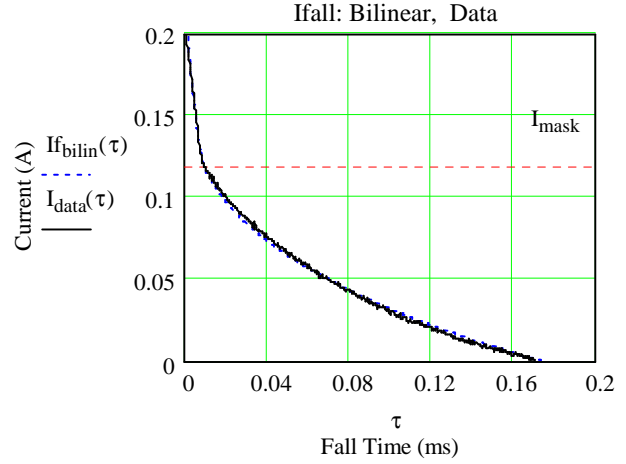Fig. 7. Skip shift solenoid @26V "linearized" current.

Fig. 8. A/C clutch relay bilinear current.

3.) Bilinear Saturation Model: We have transformed the single curve with an energy ratio of 0.35 into two curves, with ratios greater than 0.5, which are more accurately simulated with our linear model. We now form the partitioned, five point match, Bilinear Saturation Model current, $If_{bilin}(t)$, to simulate our original data. For time less than t_{mask}, the model for our original current data is $i_\Lambda(\Lambda o_H, k_H, t_{mask}, t) + I_{mask}$ and for time greater than t_{mask} the model is $i_\Lambda(\Lambda o_L, k_L, tfall - t_{mask}, t - t_{mask})$. The $\Lambda o_H i_\Lambda(t)$ plot captures the fully saturated region. The results of this procedure for the skip shift solenoid and the A/C clutch relay of Figures 5 and 6, respectively, are shown in Figures 7 and 8. As the plots reveal, linear current partitioning of the data gives an accurate representation of the original nonlinear/complex saturation current data.

VII. CONCLUSIONS

Simple electromechanical actuators display a highly saturated, linear, dynamic inductance behavior. Based upon the empirical observation that $\Lambda(i)$ can be approximated by $\Lambda o – k i$, a compact analytic solution for linear dynamic saturation was derived. The characterization parameter, Λo, can be extracted from a three-point match, using either a single central current point or the fall energy, plus the two fall current endpoints. Within the linear domain, in general, half of the high current model points are within about two percent of the current data. A Bilinear Saturation Model can be used for more accurate or complex simulations.

NOMENCLATURE

E_m	Energy dissipated in the voltage clamp measured during the fall time.
E_{tm}	Energy calculated by integral of $Vz * i_\Lambda(\Lambda o_{tm}, ko_{tm}, t_{fall}, t)$ over t_{fall}.
I_{peak}, Ipk	Peak fall current. Value of current at MOSFET turnoff (trigger point).
I_m	Fall current data point, $I_m@t_m$, used to calculate Λo_{tm}. See Appendix.
I_{mask}	Current level subtracted from high current data- mask low current region.
$i_{\Lambda H}$	High current region solution to data with a masking current subtracted.
$i_{\Lambda L}$	Low current region solution for data starting at the masking current.
k	Slope of the dynamic inductance with fall current. See Appendix.
k_{Em}	Value of k calculated from Λo_{Em}. See Appendix.
k_{tm}	Value of k calculated from Λo_{tm}. See Appendix.
L_{Ipk}, R_{Ipk}	Bi-effective inductance and resistance of the fully saturated region.
L_{tail}, R_{tail}	Bi-effective inductance and resistance of the low current tail region.
n	Exponent for power function ($Ipk\{1-(t/t_{fall})^n\}$) match to fall current. Falloff of the power function (di/dt) near t_{fall}, normalized to $Ipeak/t_{fall}$. Energy ratio: $(\text{Peak Energy}/E_m - 1)^{-1}$. See Appendix.
n_{Em}	Value of n calculated from E_m. "Effective" value. See Appendix.
n_{tm}	Value of n calculated from a current data point $I_m@t_m$. See Appendix.
R_{series}, Rs	Coil plus FET clamp resistance. If Rds_{on} is negligible $\sim V_{Bat}/Ipk$. FET clamp resistance $= \delta Vds_{clamp}/\delta Ids$, is normally a fraction of Rds_{on}, and can generally be ignored.
t_{fall}, tf	Measured fall time. Time interval between current at Ipk and zero.
t_m	Fall time data point, $t_m@I_m$ used to calculate Λo_{tm}. See Appendix.
t_{mask}	Time corresponding to current level I_{mask}. Fall time for I_{mask}.
$tfall_{encoded}$	The measured value of t_{fall} can be extracted from Λo and k. Appendix.
V_{Bat}, Vb	Average supply voltage.
Vds_{clamp}, Vz	The clamp voltage. If not constant, energy-averaged clamp voltage.
Λ	Dynamic inductance. Defined as $d\Phi_{tot}/di$. Measured as emf/di/dt.
Λ_{Ipk}	Dynamic inductance at peak current. Calculated as $\Lambda o - k\, Ipk$.
Λo	Dynamic inductance intercept at zero current. Used to characterize Λ.
Λo_{Em}	Λo calculated by matching fall energy, E_m. See Appendix.
Λo_{Em-tm}	Approximation for Λo_{Em} calculated from Λo_{tm}. See Appendix.
Λo_{tm}	Λo calculated by matching fall current at $t_m@I_m$. See Appendix.
Λo_{zpk}	Value of Λo if saturation $\sim 100\%$, i.e., $\Lambda_{Ipk} = 0$. See Appendix.

Note: The Mathcad files and data used in the development and preparation of the paper are available from the author upon request.

Appendix

Shorten variables names: $Vb = V_{Bat}$ $\qquad$ $Vz = Vds_{Clamp}$ $\qquad$ $Ipk = Ipeak$ $\qquad$ $Rs = Rseries$ $\qquad$ $tf = t_{fall}$

Effective conventional inductance given measured energy, Em

$$L_{effective} = \frac{Em * Rs^2}{Vz} * \left[Ipk * Rs + (Vz - Vb) * \ln\left(\frac{Vb}{Vz + Ipk * R - Vb}\right) \right]^{-1} \qquad (5)$$

Exponent n for Energy or Im@tm match

$$n_{Em} = \frac{Em}{Ipk * Vz * tf - Em} \qquad (6)$$

$$n_{tm} = \frac{\ln\left(1 - \frac{I_m}{Ipk}\right)}{\ln\left(\frac{t_m}{tf}\right)} \qquad (7)$$

General expression for slope, k in terms of Λo and tf

$$k(\Lambda o, tf) = \frac{2 * \left(\Lambda o * Ipk - \left(Vz - Vb + RsIpk * \frac{h}{n+1}\right) * tf\right)}{Ipk^2} \qquad (8)$$

Tfall is encoded into Λo and k

$$tfall_{encoded}(\Lambda o) = \frac{(2 * \Lambda o - k * Ipk) * Ipk}{2 * \left(Vz - Vb + Rs * Ipk * \frac{n}{n+1}\right)} \qquad (9)$$

Find Lo given a central match point Im@time=tm, clamp variables and fall time

$$\Lambda o_{tm}(I_m, t_m, tf) := \frac{a(I_m, t_m, tf) + b(I_m, t_m)}{Ipk \cdot I_m \cdot (Ipk - I_m)} \qquad (10)$$

$$a(I_m, t_m, tf) := (Vz - Vb) \cdot \left[(tf - t_m) \cdot Ipk^2 - tf \cdot I_m^2 \right] \qquad (11)$$

$$b(I_m, t_m, tf) := \left[\left[tf - \left[2 - \frac{1}{n} \cdot \left(\frac{t_m}{tf}\right)^n \right] \cdot t_m \right] \cdot Ipk^2 - tf \cdot I_m^2 \right] \cdot \frac{n \cdot Rs \cdot Ipk}{n + 1} \qquad (12)$$

REFERENCES

[1] Fields and Waves in Communication Electronic, Simon Ramo, John R. Whinnery, and Theodore van Duzer, Third Edition, John Wiley & Sons, Inc., 1994.

[2] N. Doinikov, V. Kukhtin, E. Lamzin, B. Mingalev, Yu. Severgin, S. Sytchevsky, "The Computation of the Dynamic Inductance of Magnet Systems and Force Distribution in Ferromagnetic Region on the Basis of 3-D Numerical Simulation of Magnetic Field", Particle Accelerator Conference, 1995, vol. 4, pp. 2359-2360.

[3] C. D. Manning, M. A. Halim, "New Dynamic Inductance Concept and it Application to Synchronous Machine Modeling", Electric Power Applications, IEE Proceedings, vol. 135, Sept., 1988, pp. 231- 239.

[4] CRC Standard Mathematical Tables and Formulae, 31st Edition, CRC Press, 2002, forms 27 and 30.

[5] http://mathworld.wolfram.com/LambertW-Function.html

[6] Coddington and Levinson, Theory of Ordinary Differential Equations, McGraw-Hill, 1955.

[7] D. Farenc, G. Charitat, P. Dupuy, T. Sicard, I. Pages, P. Rossel, "Clamped Inductive Switching of LDMOST for Smart Power IC's," in Proceedings of 1998 Symposium on Power Semiconductor Devices & Ics, Kyoto, Japan, 1998, pp. 3-6.